*Inorg. Chem.* **2008**, *47*, 5787−5798

Inorganic Chemistry
Article

# Tetravalent Metal Complexation by Keggin and Lacunary Phosphomolybdate Anions

**Roy Copping,[†] Leif Jonasson,[‡] Andrew J. Gaunt,[†] Dennis Drennan,[†] David Collison,[§] Madeleine Helliwell,[§] Ross J. Pirttijarvi,[§] Chris J. Jones,[||] Anne Huguet,[†,⊥] David C. Apperley,[#] Nikolas Kaltsoyannis,*[,‡] and Iain May*[,†,▽]**

*Centre for Radiochemistry Research, School of Chemistry, The University of Manchester, M13 9PL, U.K., Department of Chemistry, University College London, 20 Gordon Street, London, WC1H 0AJ, U.K., School of Chemistry, The University of Manchester, Manchester, M13 9PL, U.K., Nexia Solutions, Sellafield, Seascale, Cumbria, CA20 1PG, U.K., Ecole Nationale Supérieure de Chimie de Paris, 11 rue Pierre et Marie Curie, 75231 Paris Cedex 05, France, and Department of Chemistry, University of Durham, South Road, Durham, DH1 3LE, U.K.*

Received January 21, 2008

We report the synthesis, spectroscopic and structural characterization, and computational analysis of a series of phosphomolybdate complexes with tetravalent metal cations. The reaction between $Ce^{IV}$ and $Th^{IV}$ with phosphomolybdate at the optimum pH for the stabilization of the lacunary heteropolyoxometalate anion, $[PMo_{11}O_{39}]^{7-}$, results in the formation of compounds containing the anions $[Ce(PMo_{11}O_{39})_2]^{10-}$ and $[Th(PMo_{11}O_{39})_2]^{10-}$, respectively. Single crystal X-ray diffraction analysis was performed on salts of both species, $Cs_{10}[Ce(PMo_{11}O_{39})_2]\cdot 20H_2O$ and $(NH_4)_{10}[Th(PMo_{11}O_{39})_2]\cdot 22H_2O$. In both anionic complexes the f-block metal cation is coordinated to the four unsaturated terminal lacunary site oxygens of each $[PMo_{11}O_{39}]^{7-}$ anion, yielding 8 coordinate sandwich complexes, analogous to previously prepared related complexes. Spectroscopic characterization points to the stability of these complexes in solution over a reasonably wide pH range. Density functional analysis suggests that the Ce−O bond strength in $[Ce(PMo_{11}O_{39})_2]^{10-}$ is greater than the Th−O bond strength in $[Th(PMo_{11}O_{39})_2]^{10-}$, with the dominant bonding interaction being ionic in both cases. In contrast, under similar reaction conditions, the dominant solid state $Zr^{IV}$ and $Hf^{IV}$ complexes formed contain the anions $[Zr(PMo_{12}O_{40})(PMo_{11}O_{39})]^{6-}$ and $[Hf(PMo_{12}O_{40})(PMo_{11}O_{39})]^{6-}$, respectively. In these complexes the central Group 4 d-block metal cations are coordinated to the four unsaturated terminal lacunary site oxygens of the $[PMo_{11}O_{39}]^{7-}$ ligand and to four bridging oxygens of a plenary Keggin anion, $[PMo_{12}O_{40}]^{3-}$. In addition, $(NH_4)_5\{Hf[PMo_{12}O_{40}][(NH_4)PMo_{11}O_{39}]\}\cdot 23.5H_2O$ can be crystallized as a minor product. The structure of the anion, $\{Hf[PMo_{12}O_{40}][(NH_4)PMo_{11}O_{39}]\}^{5-}$, reveals coordination of the central $Hf^{IV}$ cation via four bridging oxygens on both the coordinated $[PMo_{11}O_{39}]^{7-}$ and $[PMo_{12}O_{40}]^{3-}$ anions. Unusually, the highly charged lacunary site remains uncoordinated to the Hf metal center but instead interacts with an ammonium cation. $^{31}P$ NMR indicates that complexation of the Keggin anion, $[PMo_{12}O_{40}]^{3-}$, to $Hf^{IV}$ and $Zr^{IV}$ will stabilize the Keggin anion to a much higher pH than usually observed.

## Introduction

Polyoxometalates attract considerable interest because of their enormous structural diversity and range of actual, and potential, applications.[1] The interaction of the mono lacunary heteropolyoxotungstate anions of general formula $[XW_{11}O_{39}]^{n-}$ (where X is usually a main group element), with f-element cations (+III and +IV) have been studied extensively. Sandwich complexes, of the type first reported by Peacock and Weakley, have been known for over thirty years.[2] In this class of complex two $[XW_{11}O_{39}]^{n-}$ anions sandwich the f-element cation, with the four terminal oxygens associated with the monolacunary defect site coordinating to the central f-block metal. Typical examples of these sandwich-type complexes include $[Eu(PW_{11}O_{39})_2]^{11-}$,[3] and $[U(GeW_{11}O_{39})_2]^{12-}$,[4] with a comprehensive structural study on the $[Ln(\beta_2\text{-}SiW_{11}O_{39})_2]^{13-}$ system (where Ln = La, Ce,

* To whom correspondence should be addressed. E-mail: n.kaltsoyannis@ucl.ac.uk (N.K.), iainmay@lanl.gov (I.M.).
[†] Centre for Radiochemistry Research, School of Chemistry, The University of Manchester.
[‡] Department of Chemistry, University College London.
[§] School of Chemistry, The University of Manchester.
[||] Nexia Solutions.
[⊥] Ecole Nationale Supérieure de Chimie de Paris.
[#] University of Durham.
[▽] Current address: Chemistry Division, Inorganic Isotope and Actinide Chemistry (C-IIAC), Los Alamos National Laboratory, Mail Stop J-514, Los Alamos, New Mexico 87545.

10.1021/ic800101t CCC: $40.75 
Published on Web 06/03/2008

Sm, Eu, Gd, Tb, Yb, Lu) recently reported.[5] A series of structurally distinct polymeric complexes have been synthesized at higher $Ln^{III}$:$[XW_{11}O_{39}]^{n-}$ ratios. Complex anions structurally characterized include $[Ln\{SiW_{11}O_{39}(H_2O)_3\}_2]^{5-}$ (Ln = La or Ce),[6] $[Nd_2(SiW_{11}O_{39})(H_2O)_{11}]^{2-}$ and $[Yb(SiW_{11}O_{39})(H_2O)_2]^{5-}$,[7] and $\{[Gd(H_2O)_6][Gd(H_2O)_2(DMSO)][\alpha\text{-}SiW_{11}O_{39}]\}^{2-}$.[8] Additional structural variety has also been observed, including a mixed monolacunary ($[PW_{11}O_{39}]^{7-}$) and dilacunary ($[PW_{10}O_{38}]^{11-}$) $Ce^{IV}$ complex, $[Ce_2(PW_{10}O_{38})(PW_{11}O_{39})_2]^{17-}$,[9] and 2:2 Ln:$[SiW_{11}O_{39}]^{8-}$ complexes incorporating acetate, $[(SiW_{11}O_{39}Ln)_2(\mu\text{-}CH_3COO)_2]^{12-}$, where Ln = Gd, Yb.[10]

Because of the greater instability of lacunary heteropolyoxomolybdates, the chemistry of $[XMo_{11}O_{39}]^{n-}$ with f-element cations is not as well developed as for the tungstate-based systems. Nevertheless, a range of sandwich complexes have been prepared including $[Nd(GeMo_{11}O_{39})_2]^{13-}$ and $[Dy(SiMo_{11}O_{39})_2]^{13-}$.[11] We have recently extended this to a study of the $[Ln(PMo_{11}O_{39})_2]^{11-}$ system across the whole $Ln^{III}$ series (except Pm).[12,13] However, our attempts to prepare the $Zr^{IV}$ analogue led to the synthesis of $[Zr(PMo_{12}O_{40})(PMo_{11}O_{39})]^{6-}$, with the $Zr^{IV}$ cation coordinating to the four unsaturated oxygen atoms of $[PMo_{11}O_{39}]^{7-}$ and 4 bridging oxygen atoms of a plenary Keggin anion, $[PMo_{12}O_{40}]^{3-}$.[14] Additionally, there have been numerous recent papers on heteropolytungstate coordination to $Zr^{IV}$,[15] including the recent structural characterization of the sandwich complex $[Zr(\alpha\text{-}PW_{11}O_{39})_2]^{10-}$ and the $Hf^{IV}$ analogue.[16] Of perhaps more applied interest is the use of $[PW_{11}O_{39}]^{7-}$ as a ligand in the quantitative analysis of both $Zr^{IV}$ and $Hf^{IV}$.[17]

The ability of tetravalent zirconium to coordinate to both $[PMo_{11}O_{39}]^{7-}$ and $[PMo_{12}O_{40}]^{3-}$ is at odds with our studies with $Ln^{III}$, where only coordination to $[PMo_{11}O_{39}]^{7-}$ has been observed. In addition, the recent synthesis of $[Zr(\alpha\text{-}PW_{11}O_{39})_2]^{10-}$ indicates that the $Zr^{IV}$ cation will readily coordinate to two $[PW_{11}O_{39}]^{7-}$ anions, forming the classical sandwich complex.[16] Clearly there is something unusual about the zirconium phosphomolybdate system, and we believed that this merited further investigation. We now report the interaction between $[PMo_{11}O_{39}]^{7-}$ (and where present $[PMo_{12}O_{40}]^{3-}$) with four large tetravalent cations, $Zr^{IV}$, $Hf^{IV}$, $Ce^{IV}$, and $Th^{IV}$. As well as an experimental study, we have also turned to computational methods with the aim of gaining further insight into this system. In particular we were interested to see if density functional methods could yield useful information on large, highly anionic complexes.

## Experimental and Computational Details

**A. General Experimental Details.** ***Caution!*** *$^{232}$This a hazardous radionuclide and toxic metal, and thus, chemical manipulations should only be undertaken in an appropriate radiochemical laboratory following recognized safety procedures.* Reagent grade chemicals were obtained commercially and used without purification, while water was purified by distillation. IR spectra were obtained from a Bruker Equinox 55/Bruker FRA 106/5 spectrometer with a coherent 500 mW laser for solid-state measurements and as ca. 0.05 mol $L^{-1}$ aqueous solutions using an ATR Golden Gate attachment. Raman spectra were recorded on the same instrument in both the solid state (20 mg samples) and in aqueous solution (ca. 0.05 mol $L^{-1}$). The IR and Raman spectra were recorded with a resolution of 2 $cm^{-1}$. Elemental analysis was performed on a Carlo ERBA instruments CHNS-O EA1108 Elemental Analyzer for C, H, and N and by a Fisons Horizon Elemental Analysis ICP-OED spectrometer for Mo and Ln. $^{31}$P NMR solution spectra were recorded in $D_2O$ on a Bruker Avance 400 MHz spectrometer in 5 mm diameter NMR sample tubes and referenced against $H_3PO_4$ (85%). $^{31}$P CP-MAS NMR solid state spectra were recorded on a Varian Unity spectrometer with a 4 mm (rotor o.d.) MAS probe. Thermogravimetric analysis (TGA) were recorded on a Mettler Toledo TGA/SDTA 851$^e$ analyzer with a heating rate of 5 °C $min^{-1}$ under a constant stream of dinitrogen.

**B. Synthesis. (i) Synthesis and Physical Analysis of $Cs_{10}[Ce(PMo_{11}O_{39})_2]\cdot 17H_2O$ ($[Ce(PMo_{11}O_{39})_2]^{10-} = 1$).** A solution of phosphomolybdic acid, $H_3PMo_{12}O_{40}\cdot xH_2O$ (78%, remainder


(1) See, for example, (a) *Heteropoly and Isopoly Oxometalates*; Pope, M. T., Ed.; Springer-Verlag: Berlin, 1983. (b) *Chem. Rev.* 1998, *98*, 1−389; Baker, L. C., Glick, D. C., Eds. (special thematic issue on polyoxometalates). (c) *Polyoxometalate Chemistry: From Topology via Self-Assembly to Applications*; Pope, M. T., Müller, A., Eds.; Kluwer: Dordrecht, The Netherlands, 2001. (d) *Polyoxometalate Chemistry for Nano-Composite Design*; Yamase, T., Pope, M. T., Eds.; Kluwer: Dordrecht, The Netherlands, 2002. (e) Pope, M. T. *Compr. Coord. Chem. II* **2003**, *4*, 635. (f) Hill, C. L. *Compr. Coord. Chem. II* **2003**, *4*, 679. (g) *Polyoxometalate Molecular Science*; Borras-Almenar, J. J., Coronado, E., Müller, A., Pope, M. T., Eds.; Kluwer: Dordrecht, The Netherlands, 2004.

(2) (a) Peacock, R. D.; Weakley, T. J. R. *J. Chem. Soc. A* **1971**, 1836. (b) Peacock, R. D.; Weakley, T. J. R. *J. Chem. Soc. A* **1971**, 1973.

(3) Zhang, C.; Howell, R. C.; Scotland, K. B.; Perez, F. G.; Todaro, L.; Francesconi, L. C. *Inorg. Chem.* **2004**, *43*, 7691.

(4) Tourne, C. M.; Tourne, G. F. *Acta Crystallogr.* **1980**, *B36*, 2012.

(5) Bassil, B. S.; Dickman, M. H.; von der Kammer, B.; Kortz, U. *Inorg. Chem.* **2007**, *46*, 2452.

(6) Sadakane, M.; Dickman, M. H.; Pope, M. T. *Angew. Chem., Int. Ed. Engl.* **2000**, *39*, 2914.

(7) Mialane, P.; Lisnard, L.; Mallard, A.; Marrot, J.; Antic-Fidancev, E.; Aschehoug, P.; Vivien, D.; Sécheresse, F. *Inorg. Chem.* **2003**, *42*, 2102.

(8) Wang, J.; Zhao, J.; Niu, J. *J. Coord. Chem.* **2006**, *59*, 1565.

(9) Sousa, F. L.; Almeida Paz, F. A.; Cavaleiro, A. M. V.; Klinowski, J.; Nogueira, H. I. S. *Chem. Commun.* **2004**, 2656.

(10) Mialane, P.; Dolbecq, A.; Riviére, E.; Marrot, J.; Sécheresse, F. *Eur. J. Inorg. Chem.* **2004**, 33.

(11) (a) Shan, Y. K.; Liu, Z. X.; Wang, B. E.; Jin, Z. S.; Wei, G. C.; Liu, Y. S. *Jiegou Huaxue* **1990**, *9*, 159. (b) Wang, E. B.; Shan, Y. K.; Zu, Z. X.; Liu, J. F.; Zhang, B. G. *Acta. Chim. Sin.* **1991**, *49*, 774. (c) Shan, Y. K.; Liu, Z. X.; Jin, Z. S.; Wei, G. C. *Acta. Chim. Sin.* **1992**, *50*, 357.

(12) Gaunt, A. J.; May, I.; Sarsfield, M. J.; Collison, D.; Helliwell, M.; Dennis, I. S. *Dalton Trans.* **2003**, 2767.

(13) Copping, R.; Gaunt, A. J.; May, I.; Sarsfield, M. J.; Collison, D.; Helliwell, M.; Dennis, I. S.; Apperley, D. C. *Dalton Trans.* **2005**, 1256.

(14) Gaunt, A. J.; May, I.; Collison, D.; Fox, O. D. *Inorg. Chem.* **2003**, *42*, 5049.

(15) See, for example, (a) Chauveau, F.; Eberle, J.; Lefebvre, J. *J. Nouv. J. Chim.* **1985**, *9*, 315. (b) Finke, R. G.; Rapko, B.; Weakley, T. J. R. *Inorg. Chem.* **1989**, *28*, 1573. (c) Gaunt, A. J.; May, I.; Collison, D.; Holman, K. T.; Pope, M. T. *J. Mol. Struct.* **2003**, *656*, 101. (d) Villanneau, R.; Carabineiro, H.; Carrier, X.; Thouvenot, R.; Herson, P.; Lemos, F.; Ribeiro, F. R.; Che, M. *J. Phys. Chem. B* **2004**, *108*, 12456. (e) Fang, X.; Anderson, T.; Hill, C. *Chem. Commun.* **2005**, 5044. (f) Fang, X.; Anderson, T.; Hill, C. L. *Angew. Chem., Int. Ed.* **2005**, *44*, 3540. (g) Bassil, B. S.; Dickman, M. H.; Kortz, U. *Inorg. Chem.* **2006**, *45*, 2394. (h) Kholdeeva, O. A.; Maksimov, G. M.; Maksimovskaya, R. I.; Vanina, M. P.; Trubitsina, T. A.; Naumov, D. Yu.; Kolesov, B. A.; Antonova, N. S.; Carbó, J. J.; Poblet, J. M. *Inorg. Chem.* **2006**, *45*, 7224.

(16) (a) Kato, C. N.; Shinohara, A.; Hayashi, K.; Nomiya, K. *Inorg. Chem.* **2006**, *45*, 8108. (b) Sokolov, M. N.; Chubarova, E. V.; Peresypkina, E. V.; Virovets, A. V.; Fedin, V. P. *Russ. Chem. B., Int. Ed.* **2007**, *56*, 220.

(17) Himeno, S.; Kitano, E.; Chaen, N. *Electrophoresis* **2007**, *28*, 1525.

moisture, 2 mmol, 4.68 g) in $H_2O$ (40 mL) was adjusted to pH 4.3 by the addition of small solid portions of $Li_2CO_3$ (maximum 50 mg per portion), which dissolved on stirring. $(NH_4)_2Ce(NO_3)_6$ solution (1 mL, 1 mmol) was added to the yellow solution and the pH dropped to 1.8. The pH was then raised back to 4.3 by further additions of $Li_2CO_3$ and the solution stirred for 1 h. $Cs_2CO_3$ (10.7 mmol, 3.50 g) was added to the solution with stirring, resulting in the immediate formation of a yellow precipitate and the pH of the slurry increased slightly to 4.6. A few drops of 0.1 mol $L^{-1}$ HCl was added to reduce the pH of the slurry back to 4.3, which was then stirred for 30 min. The yellow solid was collected by vacuum filtration, washed with cold water (2 × 5 mL), and allowed to air-dry overnight (yield 4.80 g, 92%). A 1 g portion of the solid was then stirred vigorously in $H_2O$ (150 mL) for 1 h, which dissolved some of the solid product. The yellow suspension was then centrifuged, and the yellow supernatant collected. Crystals suitable for single crystal X-ray diffraction were grown by vapor diffusion of the resultant solution with hexane over several weeks. The bulk solid appeared analogous to the single crystals by comparison of IR and Raman spectra. Calculated (found) (%) for $Cs_{10}[Ce(PMo_{11}O_{39})_2]\cdot 17H_2O$: H 0.70 (0.60), P 1.19 (1.23), Mo 40.48 (39.75), Ce 2.69 (2.86). The TGA curve was obtained between 25 and 900 °C and revealed a weight loss of 6.2% up to 250 °C in two steps corresponding to the loss of 17 $H_2O$ molecules that are assigned in the formula. The initial loss of water molecules corresponds to those that are only weakly bound in the lattice and the second step to tightly bound water molecules of crystallization. It is also possible that in this temperature range the trace quantity of carbonate found in the product could be lost as $CO_2$. No further mass drop is observed until about 800 °C where a small decrease is observed up to the ceiling temperature of 900 °C. This could be attributed to a start in the reduction of molybdenum to molybdenum metal via a possible $N_2$ reduction pathway, with a brownish-gray residual solid remaining.

**(ii) Synthesis and Physical Analysis of $(NH_4)_{10}[Ce(PMo_{11}O_{39})_2]\cdot 23.4H_2O$ - $[Ce(PMo_{11}O_{39})_2]^{10-}$ = 1.** This compound was synthesized in an analogous manner to the previously reported hydrated ammonium salts of $[Ln^{III}(PMo_{11}O_{39})_2]^{11-}$, using $(NH_4)_2Ce(NO_3)_6$ (0.548 g, 1.00 mmol) as the source of $Ce^{IV}$ and EtOH to aid crystallization (yield 2.11 g, 51%).[12,13] Calculated (found) (%) for $(NH_4)_{10}[Ce(PMo_{11}O_{39})_2]\cdot 23.4H_2O$: H 2.11 (1.78), N 3.37 (3.49), P 1.49 (1.64), Mo 50.70 (51.94), Ce 3.37 (3.35). TGA analysis indicated the presence of 23.4 molecules of $H_2O$. Spectroscopically (Raman/IR) this complex was identical to the hydrated Cs salt of **1**, but crystals suitable for X-ray diffraction could not be grown.

**(iii) Synthesis and Physical Analysis of $(NH_4)_{10}[Th(PMo_{11}O_{39})_2]\cdot 27H_2O$ - $[Th(PMo_{11}O_{39})_2]^{10-}$ = 2.** A solution of phosphomolybdic acid, $H_3PMo_{12}O_{40}\cdot xH_2O$ (78%, remainder moisture) (2 mmol, 4.68 g) in $H_2O$ (40 mL) was adjusted to pH 4.3 by the addition of small solid portions of $Li_2CO_3$, which dissolved with magnetic stirring. $Th(NO_3)_4\cdot 6H_2O$ (1 mmol, 0.61 g) was added to the yellow solution and dissolved with magnetic stirring, resulting in a pH drop to 2.0. The pH was then raised back to 4.3 by further additions of $Li_2CO_3$ (maximum 50 mg per addition) and the solution stirred for 1 h. before small traces of residual solid were removed by centrifugation. $NH_4Cl$ (22 mmol, 1.17 g) was added to the yellow solution and dissolved with a minor decrease in pH noted. The solution was divided into two equal portions and to one-half EtOH was added dropwise until it was no longer immediately miscible with swirling and the solution stored in a refrigerator at 5 °C for 1 week. This yielded a yellow semicrystalline material, which was collected by vacuum filtration, washed with cold water, and air-dried (1.51 g, 70% yield). Yellow plate-like crystals suitable for X-ray diffraction were grown by addition of a few drops of EtOH to the other half of the solution and storage at 5 °C for several weeks and appeared analogous to the bulk solid by comparison of IR and Raman spectra. Calculated (found) (%) for $(NH_4)_{10}[Th(PMo_{11}O_{39})_2]\cdot 27H_2O$: H 2.19 (2.11), N 3.24 (3.36), P 1.43 (1.54), Mo 48.86 (48.46), Th 5.37 (5.06). The TGA curve between 25 and 900 °C revealed a mass loss of 12% between 25 and 250 °C corresponding to about 27 water molecules that are assigned to the formula. Between 250 and 420 °C there was a further 4.5% reduction in weight corresponding to 10.7 $NH_3$ molecules that originate from the decomposition of $NH_4^+$ cations and is in reasonable agreement with the number of ammonium counter-cations associated with the anionic complex. There was no further weight loss up to 700 °C after which there was a steep decrease in weight loss up to the instruments ceiling temperature of 900 °C, likely because of the reduction of molybdenum to molybdenum metal by $N_2$ and the concomitant loss of oxygen. A gray residue in the crucible at the end of the experiment could signify the presence of molybdenum metal.

**(iv) Synthesis of $(NH_4)_6[Hf(PMo_{11}O_{39})(PMo_{12}O_{40})]\cdot 22H_2O$ - $[Hf(PMo_{11}O_{39})(PMo_{12}O_{40})]^{6-}$ = 3a and $(NH_4)_5\{Hf[PMo_{12}O_{40}][(NH_4)PMo_{11}O_{39}]\}\cdot 23.5H_2O$ - $\{Hf[PMo_{12}O_{40}][(NH_4)PMo_{11}O_{39}]\}^{5-}$ = 3b (where a = bulk solid and b = single crystals).** Phosphomolybdic acid (78%, remainder moisture, 2 mmol, 4.68 g) was dissolved in distilled $H_2O$ (40 mL), and the pH adjusted to 4.3 by the addition of small portions of $Li_2CO_3$ with stirring. $HfCl_4$ (1 mmol, 0.32 g), dissolved in distilled water (5 mL) was added to the yellow solution with stirring and the pH dropped to about 2. The pH was then raised back to 4.3 by further addition of $Li_2CO_3$ (50 mg max. per addition) and the solution stirred for 1 h. $NH_4Cl$ (28 mmol, 1.5 g) was added to the solution, which was then stirred for a further 20 min. EtOH was added dropwise to the solution with swirling until it was no longer immediately miscible, and the solution stored in a refrigerator for one week yielding a yellow powder, which was collected by vacuum filtration, washed with cold water (2 × 5 mL), and air-dried (2.09 g, 50% yield) - complex **3a**. The analogous $Zr^{IV}$ complex (**4a**) was prepared the same way using $ZrCl_4$. Crystals suitable for single crystal X-ray diffraction were grown by adding a few drops of MeOH to a small (~2 mL) portion of the bulk solution and stored at 5 °C for several days. Small yellow plate-like crystals in low yield were separated from a yellow precipitate and appeared different from the bulk powder by IR spectroscopy. A small quantity of block-like crystalline material, with an IR spectrum similar to that of the plate crystals, was also grown by diffusion of MeOH into a small portion of the bulk solution and these appeared structurally identical to the plate-like crystals by single crystal X-ray diffraction (complex **3b**). Elemental analysis was determined on a bulk powder sample obtained prior to crystallization. Calculated. (found) (%) for $(NH_4)_6[Hf(PMo_{11}O_{39})(PMo_{12}O_{40})]\cdot 22H_2O$ (**3a**): H 1.63 (1.74), N 1.99 (2.49), P 1.47 (1.61), Mo 52.34 (51.18), Hf 4.23 (4.47), Cl 0 (0.21). The high found value obtained for % N can in part be attributed to $NH_4Cl$ impurity, consistent with the slightly higher % H and % Cl values. The TGA curve for the bulk powder sample of **3a** between 25 and 900 °C revealed a weight loss of 10.5% between 25 and 250 °C corresponding to the loss of about 22 water molecules that are assigned to the formula. Between 250 and 400 °C there is a further 3.9% loss in weight corresponding to about 10 $NH_3$ molecules from the decomposition of $NH_4^+$. This is a greater level than anticipated, probably because of the compound containing excess ammonium chloride, as indicated from the elemental analysis results. The compound was stable up to 700 °C after which a sharp decrease in weight loss was observed, similar

to the TGA curves of **1** and **2**, and again attributed to the formation of molybdenum metal and the concomitant loss of oxygen.

**C. Crystallographic Studies.** All structures were solved and refined using SHELXTL (G.M. Sheldrick, SHELX97, University of Göttingen, Germany, 1997).

**Crystal data for $Cs_{10}[Ce(PMo_{11}O_{39})_2]\cdot 20H_2O$.** Chemical formula = $H_{40}CeCs_{10}Mo_{22}O_{98}P_2$, Mw = 5250.16, monoclinic space group, *C*2/*c*, $a = 37.7066(15)$ Å, $b = 13.3093(5)$ Å, $c = 19.9971(7)$ Å, $\alpha = 90°$, $\beta = 118.149(6)°$, $\gamma = 90°$, $V = 8848.5(6)$ Å$^3$, $T = 100(2)$ K, $Z = 4$, Oxford Diffraction Crysalis CCD diffractometer ($\lambda = 0.71073$ Å), $\mu = 7.727$ mm$^{-1}$, crystal dimensions = 0.20 × 0.10 × 0.05 mm, 45889 reflections measured, 14305 of which were unique (R(int) = 0.0378) 11633 with $I > 2\sigma(I)$. The structure was solved by direct methods, with all of the non-H atoms refined anisotropically. The asymmetric unit contains half the cluster, 5 $Cs^+$ ions and 10 water molecules. Final R ($I > 2\sigma(I)$), R1 = 0.0425, wR2 = 0.0974. Final R (all data), R1 = 0.0590, wR2 = 0.1036.

**Crystal data for $(NH_4)_{10}[Th(PMo_{11}O_{39})_2]\cdot 22H_2O$.** Chemical formula = $H_{84}Th_1Mo_{22}N_{10}O_{100}P_2$, Mw = 4229.43, monoclinic space group, *C*2/*c*, $a = 37.507(7)$ Å, $b = 13.024(3)$ Å, $c = 19.543(4)$ Å, $\alpha = 90°$, $\beta = 117.665(3)°$, $\gamma = 90°$, $V = 8455(3)$ Å$^3$, $T = 100(2)$ K, $Z = 4$, Bruker Smart Platform CCD, Mo Kα radiation ($\lambda = 0.71073$ Å), $\mu = 5.077$ mm$^{-1}$, crystal dimensions = 0.10 × 0.05 × 0.05 mm, 31840 reflections measured, 8553 of which were unique (R(int) = 0.0880) 7030 with $I > 2\sigma(I)$. The structure was solved by direct methods, with a number of the oxygen and nitrogen atoms treated isotropically. The asymmetric unit contains half the cluster, 5 $NH_4^+$ ions and 11 water molecules. Final R ($I > 2\sigma(I)$), R1 = 0.1395, wR2 = 0.3721. Final R (all data), R1 = 0.1520, wR2 = 0.3767.

**Crystal data for $(NH_4)_5\{Hf[PMo_{12}O_{40}][(NH_4)PMo_{11}O_{39}]\}\cdot 23.5H_2O$.** Chemical formula = $H_{71}Hf_1Mo_{23}N_6O_{102.5}P_2$, Mw = 4242.68, monoclinic space group, $P2_1/c$, $a = 13.3813(6)$ Å, $b = 37.9050(11)$ Å, $c = 20.5948(8)$ Å, $\alpha = 90°$, $\beta = 114.223(3)°$, $\delta = 90°$, $V = 9526.3(6)$ Å$^3$, $T = 100(2)$ K, $Z = 4$, Oxford Diffraction Crysalis CCD diffractometer, Mo Kα radiation ($\lambda = 0.71073$ Å), $\mu = 4.142$ mm$^{-1}$, crystal dimensions = 0.15 × 0.10 × 0.05 mm, 47173 reflections measured, 17086 of which were unique (R(int) = 0.0395) 13351 with $I > 2\sigma(I)$. The structure was solved by direct methods. The asymmetric unit contains the cluster, 6 $NH_4^+$ ions, and 23.5 water molecules. All of the non-H atoms were refined anisotropically except for the oxygen atoms of the solvent water molecules. Ammonium counter-ions were distinguished from water molecules by first treating all the non hydrogen atoms surrounding the polyoxometalate complex as oxygens and then by assigning those with highest thermal parameters as nitrogens. Final R ($I > 2\sigma(I)$), R1 = 0.0689, wR2 = 0.1700. Final R (all data), R1 = 0.0878, wR2 = 0.1784.

**D. Solution $^{31}$P NMR Studies as a Function of pH.** In a typical experiment, phosphomolybdic acid, $H_3PMo_{12}O_{40}$ (78%, remainder moisture, 4.68 g, 2 mmol) was dissolved in $H_2O$ (50 mL) under constant stirring to which $Th(NO_3)_4\cdot 6H_2O$ (0.58 g, 1 mmol) dissolved in $H_2O$ (5 mL) was added. The resultant solution was allowed to stir for approximately 30 min, when all of the solid had dissolved, and the pH was recorded (0.90). A small portion of the resulting solution was collected and pipetted into a 3 mm Teflon NMR tube, which was inserted into a 5 mm glass NMR tube containing $D_2O$ as a locking solvent. The pH of the solution was then increased in about 0.4−0.7 increments by additions of $Li_2CO_3$ up to a pH of 5−6, ensuring that at each stage the solid was completely dissolved. At each pH increment a sample was collected for $^{31}$P NMR spectroscopy. A similar methodology was employed for the $Ce^{IV}$, $Hf^{IV}$, and $Zr^{IV}$ phosphomolybdate $^{31}$P NMR with $(NH_4)_2Ce(NO_3)_6$, $HfCl_4$ and $ZrCl_4$ used as the source of the $M^{IV}$ cations.

**E. Computational Details.** All calculations were performed with the ADF2006.01b suite of programs.[18] Uncontracted, STO basis sets of TZ2P quality were employed, in conjunction with the frozen core approximation (O·1s, P·2p, Zr·3d, Mo·3d, Hf·4d, W·4d, Ce·4d, and Th·5d). The Zero Order Regular Approximation (ZORA) to the Dirac equation was used to account for scalar relativistic effects in all calculations.[19]

Geometry optimizations were performed on **1** and **2** in the $C_2$ point group, using the crystallographic coordinates as initial guesses. The integration parameter was set to 3.0 and the self-consistent field (SCF) and energy gradient convergence criteria were employed at the ADF default settings ($10^{-6}$ and $10^{-2}$ H Å$^{-1}$, respectively). The local density parametrization of Vosko, Wilk, and Nusair was employed in all geometry optimizations.[20] Single point calculations were performed at the optimized geometries using the PBE GGA exchange-correlation functional.[21]

PBE single point calculations were performed on $[M(PMo_{11}O_{39})(PMo_{12}O_{40})]^{6-}$ (M = Zr, Hf). For both the Zr and Hf systems, the crystallographic coordinates of $[Zr(PMo_{11}O_{39})(PMo_{12}O_{40})]^{6-}$ (**4a**) were employed.[14] To obtain SCF convergence for these single point calculations, it was necessary to employ an electron smearing factor, that is, a pseudothermal distribution function was used to distribute the electron occupations fractionally over a few states around the highest occupied molecular orbital (HOMO). It was not possible to reduce the smearing factor below 3 mH for $[Zr(PMo_{11}O_{39})(PMo_{12}O_{40})]^{6-}$ and 4 mH for $[Hf(PMo_{11}O_{39})(PMo_{12}O_{40})]^{6-}$, resulting in noninteger occupations of a few molecular orbitals around the HOMO, but the results (atomic charges, bond energy analyses) were found to vary very little with these small smearing factors.

For **3b** and the corresponding proposed Zr complex, **4b**, the crystallographic coordinates of **3b**, $\{Hf[PMo_{12}O_{40}][(NH_4)PMo_{11}O_{39}]\}^{5-}$, were employed with the addition of four hydrogen atoms, optimized (using the local density parametrization of Vosko, Wilk, and Nusair) without symmetry constraints to chemically sensible positions around the nitrogen atom in the lacunary cavity. A smearing value of 1 mH was employed for these partial geometry optimizations of the H atoms in **3b** and **4b**, and the same value was used for subsequent PBE single points.

Partial atomic charges have been calculated using the Mulliken, Voronoi, and Hirshfeld schemes. Mulliken atomic populations, and Mayer Bond Orders,[22] are also reported.


(18) Baerends, E. J.; Autschbach, J.; Bérces, A.; Bickelhaupt, F. M.; Bo, C.; Boerrigter, P. M.; Cavallo, L.; Chong, D. P.; Deng, L.; Dickson, R. M.; Ellis, D. E.; van Faassen, M.; Fan, L.; Fischer, T. H.; Fonseca Guerra, C.; van Gisbergen, S. J. A.; Groeneveld, J. A.; Gritsenko, O. V.; Grüning, M.; Harris, F. E.; van den Hoek, P.; Jacob, C. R.; Jacobsen, H.; Jensen, L.; van Kessel, G.; Kootstra, F.; van Lenthe, E.; McCormack, D. A.; Michalak, A.; Neugebauer, J.; Osinga, V. P.; Patchkovskii, S.; Philipsen, P. H. T.; Post, D.; Pye, C. C.; Ravenek, W.; Ros, P.; Schipper, P. R. T. Schreckenbach, G.; Snijders, J. G.; Solà, M.; Swart, M.; Swerhone, D.; te Velde, G.; Vernooijs, P.; Versluis, L.; Visscher, L.; Visser, O.; Wang, F.; Wesolowski, T. A.; van Wezenbeek, E.; Wiesenekker, G.; Wolff, S. K.; Woo, T. K.; Yakovlev, A. L.; Ziegler, T. *ADF 2006. 01, SCM*; Theoretical Chemistry, Vrije Universiteit: Amsterdam, The Netherlands; http://www.scm.com.

(19) van Lenthe, E.; Baerends, E. J.; Snijders, J. G. *J. Chem. Phys.* **1993**, *99*, 4597.

(20) Vosko, S. H.; Wilk, L.; Nusair, M. *Can. J. Phys.* **1980**, *58*, 1200.

(21) Perdew, J. P.; Burke, K.; Enzerhof, M. *Phys. Rev. Lett.* **1997**, *77*, 3865.

(22) Bridgeman, A. J.; Cavigliasso, G.; Ireland, L. R.; Rothery, J. *J. Chem. Soc., Dalton Trans.* **2001**, 2095.

ADF defines the total bonding energy as the energy difference between the molecular fragments in their final positions and at infinite separation. These molecular fragments may be individual atoms or groups of atoms, and for a discussion of the use of fragments within ADF, the reader is directed to a previous detailed description.[23] These fragments are placed at their positions within the molecule. At this point there is an electrostatic interaction between them, comprising the nucleus/nucleus, nucleus/electron and electron/electron Coulombic interactions. This electrostatic interaction is computed from the unperturbed and superimposed charge densities of the separate fragments. Next it is ensured that the overall molecular wave function satisfies the Pauli principle. This is done by requiring that the one-electron orbitals of the combined fragments form a correct single-determinantal wave function. However, it is extremely unlikely that this will be the case for the fragment orbitals when the fragments are simply placed at their positions within the molecule because the orbitals on the different fragments will not be orthogonal to one another. Thus, the next step is to orthogonalize the occupied fragment orbitals to obtain a correct single-determinantal, antisymmetrised molecular wave function. This will result in a change in the molecular charge density, and the accompanying energy change is known as the Pauli, or exchange, repulsion. The final part of the process is to allow the fragment orbitals to relax to self-consistency, and the interaction energy between the orbitals of the various fragments is defined as the electronic (or orbital) interaction.[24]

For **1** and **2**, a two-fragment approach was employed using the PBE functional at the optimized geometries; $M^{4+}$ and $(PMo_{11}O_{39})_2^{14-}$. It was not possible to obtain SCF convergence for the Zr and Hf systems using a two-fragment approach; hence, energy decomposition data for these compounds were obtained from three fragments; $M^{4+}$ + $PMo_{12}O_{40}^{3-}$ + $PMo_{11}O_{39}^{3-}$, including $NH_4^+$ where relevant. Electron smearing was required to obtain converged SCFs for these fragment calculations, 0.6 mH for $[Zr(PMo_{11}O_{39})(PMo_{12}O_{40})]^{6-}$ - **4a** and 0.9 mH for $Hf(PMo_{11}O_{39})(PMo_{12}O_{40})^{6-}$ - **3a**. Fragment calculations on **3b** and **4b** were unsuccessful.

## Results and Discussion

**A. Cerium(IV) and Thorium(IV) Systems. (i) Structures of $Cs_{10}[Ce(PMo_{11}O_{39})_2]\cdot 20H_2O$ and $(NH_4)_{10}[Th(PMo_{11}O_{39})_2]\cdot 22H_2O$, and Computational Analysis of the Metal−POM Interactions.** Diffraction data were collected for both $Cs_{10}[Ce(PMo_{11}O_{39})_2]\cdot 20H_2O$ and $(NH_4)_{10}[Th(PMo_{11}O_{39})_2]\cdot 22H_2O$. A total of 20 and 22 water molecules of crystallization were assigned in crystallographic characterization of the $Ce^{IV}$ and $Th^{IV}$ complexes, respectively, which is in reasonable agreement with the values assigned after TGA considering that moisture can either be lost or gained in the bulk product.

Both the $[Ce(PMo_{11}O_{39})_2]^{10-}$ (**1**) and $[Th(PMo_{11}O_{39})_2]^{10-}$ (**2**) sandwich complexes crystallize in the *C*2/*c* monoclinic space group and are structurally identical. Both $Ce^{IV}$ and $Th^{IV}$ occupy an eight coordinate position sandwiched between two $[PMo_{11}O_{39}]^{7-}$ anions and are bonded through four terminal unsaturated oxygen atoms of each polyoxoanion. The *C*2/*c* space group has a 2-fold rotation symmetry operation, which generates the second half of the structure from the asymmetric unit cell. Oak Ridge Thermal Ellipsoid Plot (ORTEP) and polyhedral representations of the complexes are given in Figures 1 and 2, respectively, which are isostructural with the Ln series that we have reported previously.[12,13] The geometry around the central metal in each complex is square antiprismatic as determined by applying Haigh's rules.[25]

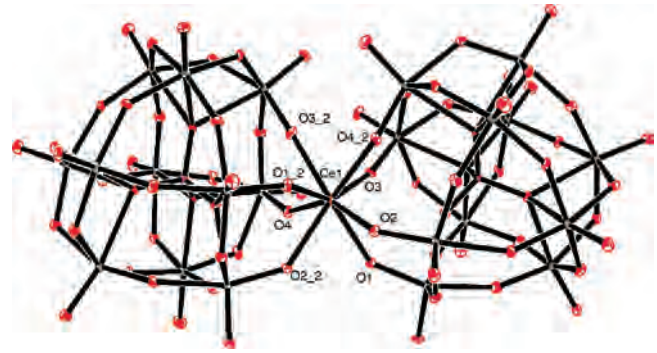


**Figure 1.** ORTEP representation (50% probability ellipsoids) of **1**.

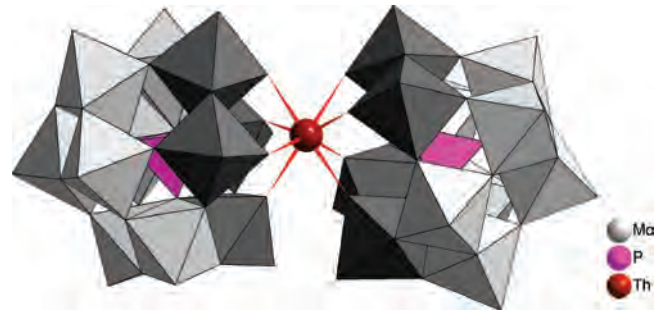


**Figure 2.** Polyhedral representation of **2**, the darker shaded polyhedrons represent the Mo octahedra that have associated terminal unsaturated oxygen atoms.

**Table 1.** $M^{4+}-O_{terminal}$ Bond Length for $[Ce(PMo_{11}O_{39})_2]^{10-}$ (**1**) and $[Th(PMo_{11}O_{39})_2]^{10-}$ (**2**); Calculated Values in Italics

| | distances (Å) | |
|---|---|---|
| bond | $[Ce(PMo_{11}O_{39})_2]^{10-}$ | $[Th(PMo_{11}O_{39})_2]^{10-}$ |
| $M^{4+}-O1$ | 2.336(4), *2.439* | 2.416(2), *2.442* |
| $M^{4+}-O2$ | 2.373(4), *2.414* | 2.453(3), *2.477* |
| $M^{4+}-O3$ | 2.309(4), *2.374* | 2.392(3), *2.436* |
| $M^{4+}-O4$ | 2.305(4), *2.334* | 2.377(3), *2.463* |
| "short" $M^{4+}-O$ average | 2.307, *2.354* | 2.385, *2.439* |
| "long" $M^{4+}-O$ average | 2.355, *2.423* | 2.435, *2.470* |
| average | 2.33, *2.390* | 2.41, *2.454* |

The experimental and computed $M^{IV}-O$ bond distances for **1** and **2** are summarized in Table 1. The coordination sphere around the central metal cation in both complexes consists of four "long" and four "short" tetravalent metal−oxygen bonds for reasons that have previously been discussed.[12,13] The average experimental Ce−O and Th−O bond lengths are 2.33 and 2.41 Å, respectively, and this increase from Ce to Th is also observed computationally, although the computed averages are 0.06 Å (Ce) and 0.04 Å (Th) larger than experiment. The larger averages observed computationally reflect the fact that all of the computed M−O distances are longer than experiment. Generally, the LDA performs better than GGA functionals for bond lengths in

(23) Baerends, E. J.; Branchadell, V.; Sodupe, M. *Chem. Phys. Lett.* **1997**, *265*, 481.
(24) (a) Ziegler, T.; Rauk, A. *Theor. Chim. Acta.* **1977**, *46*, 1. (b) Ziegler, T.; Rauk, A. *Inorg. Chem.* **1979**, *18*, 1558.
(25) Haigh, C. W. *Polyhedron* **1995**, *14*, 2871.

**Table 2.** PBE Energy Decomposition Data (eV) for **1** ($Ce^{IV}$) and **2** ($Th^{IV}$) at Their Optimized (LDA) Geometries

| | **1** $[Ce(PMo_{11}O_{39})_2]^{10-}$ | **2** $[Th(PMo_{11}O_{39})_2]^{10-}$ |
|---|---|---|
| electrostatic | −129.08 | −128.34 |
| Pauli | 9.51 | 9.98 |
| prerelaxation (= electrostatic + Pauli) | −119.57 | −118.35 |
| orbital | −51.90 | −45.93 |
| total bonding energy | −171.47 | −164.28 |

compounds containing metals in high oxidation states with hard donor ligands,[26] with GGA approaches tending to produce bond lengths which are too long. That even the LDA in the present case overestimates the M−O distances is most likely a consequence of the very large charge on the anions.

The longer Th−O versus Ce−O, found both experimentally and computationally, reflect the ionic radii of $M^{IV}$, 0.97 Å and 1.05 for $Ce^{IV}$ and $Th^{IV}$, respectively. Interestingly, both the $Ce^{IV}$ and $Th^{IV}$ complexes have average M−O bond lengths that sit above a plot of $Ln^{III}$−O bond lengths versus ionic radii for the $[Ln(PMo_{11}O_{39})_2]^{11-}$ series of complexes (see Supporting Information). This is somewhat counter intuitive as it might be expected that the increased charge on the metal cation in the tetravalent metal complexes would result in an even stronger interaction with the ligand and a resulting closer coordination.

The smaller ionic radius of $Ce^{IV}$ compared with $Th^{IV}$, and resultant higher positive charge density, should lead to an increased M−O interaction and closer coordination by the two sandwiching lacunary anions. Both the experimental and the computed M−O distances are consistent with this expectation. Furthermore, the results of energy decomposition analyses, performed using the PBE functional at the optimized geometries, given in Table 2, indicate a significantly larger Ce−POM interaction. The dominant term for both systems is electrostatic, as expected given that the fragments are so highly charged ($M^{4+}$ and $(PMo_{11}O_{39})_2^{14-}$). This term is nearly 1 eV larger in **1** than **2**, presumably as a result of the shorter M−O. The Pauli term is slightly larger in the Th complex, and the combination of reduced electrostatic and increased Pauli term leads to the prerelaxation term being more than 1 eV less negative in **2**. As the orbital term is significantly larger in **1** than **2**, the total M−POM interaction is more than 7 eV larger in the 4f anion.

The orbital term cannot be straightforwardly associated with any single type of bonding, as it incorporates all interactions between the chosen fragments that result from relaxation of the starting electronic structure to self-consistency. Nevertheless, we were recently confidently able to associate the larger U−N versus U−O orbital interactions in calculations on $[UO_2Cl_2(Cy_3PNH)_2]$ and $[UO_2Cl_2(Cy_3PO)_2]$ with greater U−N covalency.[27] To gain further insight into the metal−POM interaction, we have calculated the Mulliken, Voronoi, and Hirshfeld partial charges of the metal atoms, and the oxygens to which they are coordinated, and these are collected in Table 3. The Mulliken charges of

**Table 3.** PBE Partial Atomic Charges for **1** ($Ce^{IV}$) and **2** ($Th^{IV}$) at the LDA Optimized Geometries

| | Mulliken | | Voronoi | | Hirshfeld | |
|---|---|---|---|---|---|---|
| | Ce | Th | Ce | Th | Ce | Th |
| O1 | −0.59 | −0.62 | −0.27 | −0.26 | −0.27 | −0.28 |
| O2 | −0.60 | −0.62 | −0.26 | −0.25 | −0.28 | −0.28 |
| O3 | −0.59 | −0.63 | −0.27 | −0.26 | −0.28 | −0.28 |
| O4 | −0.60 | −0.63 | −0.26 | −0.25 | −0.27 | −0.28 |
| M | 1.56 | 1.67 | 0.32 | 0.27 | 0.54 | 0.67 |

the oxygen atoms are all found to be quite negative, those in **2** slightly more so than in **1**, and the metal atoms rather positive. For the other charge schemes, the oxygen atoms are found to be less negative, and very similar to one another in both compounds. The metal atoms carry a positive charge in both Voronoi and Hirshfeld schemes, more so in the latter. Partial charges are rarely, if ever, calculated to be as large as formal oxidation states would suggest, and hence the >2 charge unit difference between the metal and oxygen Mulliken values is indicative of a strongly ionic interaction. Voronoi and Hirshfeld charges are typically smaller in absolute terms than Mulliken, and hence the metal−oxygen charge differences found here also suggest rather ionic bonding. Unfortunately, the three charge schemes are not in full agreement as to which metal carries the more positive charge; Mulliken and Hirshfeld indicate Th while Voronoi suggests Ce. However, we are unsure as to the significance of this difference, as the very large negative charge carried by **1** and **2** leads to many unbound molecular orbitals (i.e., occupied orbitals with positive eigenvalues). We suspect that the reliability of all three charge schemes is reduced in these circumstances, and hence that one should not to read too much into the variations of the charges between metals. It is probably best to conclude simply that all three schemes indicate significant ionicity in Ce−O and Th−O bonding in **1** and **2**, respectively.

To assess the extent to which environmental effects might alter the above conclusions, we attempted to reoptimize **1** and **2** in aqueous solution via the COSMO approach. This proceeded smoothly for **2**, but it proved impossible to obtain a satisfactorily converged geometry for **1**. The effect on the geometry of **2** was minor, the average "short", "long", and overall Th−O distances being 2.44, 2.45, and 2.45 Å, respectively. Furthermore, little difference was found between the partial charges calculated in solution and those obtained from the gas-phase calculation above. The Mulliken charges on O1−O4 are slightly more negative in solution (by about 0.08 e) and the Th charge a little more positive (1.71 *vs* 1.67 in gas phase). We therefore conclude that environmental effects, at least as considered via the COSMO approach, are rather small, and suggest a slightly greater ionic component to the Th−O bonding. Unfortunately, we cannot probe this further using an energy decomposition analysis, as this is not implemented in ADF for anything other than atomic fragments in conjunction with the COSMO.

The Mulliken atomic populations are given in Table 4. Formally, both metal ions have the configuration $ns^0np^0(n-1)d^0(n-2)f^0$, where $n = 6$ for Ce and 7 for Th. In both **1** and **2** the Mulliken p population is not significantly different from the expected one. The Ce s population is also

(26) Bray, M. R.; Deeth, R. J.; Paget, V. J.; Sheen, P. D. *Int. J. Quantum Chem.* **1997**, *61*, 85.

(27) Häller, L. J. L.; Kaltsoyannis, N.; Sarsfield, M. J.; May, I.; Cornet, S. M.; Redmond, M. P.; Helliwell, M. *Inorg. Chem.* **2007**, *46*, 4868.

**Table 4.** PBE Mulliken Population Analysis of **1** ($Ce^{IV}$) and **2** ($Th^{IV}$) at Their LDA Optimized Geometries

| | Ce | | | | Th | | | |
|---|---|---|---|---|---|---|---|---|
| | s | p | d | f | s | p | d | f |
| O1 | 1.91 | 4.65 | 0.03 | 0.0 | 1.90 | 4.69 | 0.03 | 0.0 |
| O2 | 1.91 | 4.67 | 0.03 | 0.0 | 1.90 | 4.70 | 0.03 | 0.0 |
| O3 | 1.91 | 4.65 | 0.03 | 0.0 | 1.90 | 4.70 | 0.03 | 0.0 |
| O4 | 1.91 | 4.67 | 0.03 | 0.0 | 1.90 | 4.70 | 0.03 | 0.0 |
| M | 0.03 | 0.12 | 1.25 | 1.05 | 0.24 | 0.01 | 1.28 | 0.81 |

**Table 5.** PBE Ce/Th−O Mayer Bond Orders of **1** ($Ce^{IV}$) and **2** ($Th^{IV}$) at Their LDA Optimized Geometries

| | **1** | **2** |
|---|---|---|
| O1/O5 | 0.37 | 0.39 |
| O2/O6 | 0.42 | 0.37 |
| O3/O7 | 0.39 | 0.39 |
| O4/O8 | 0.47 | 0.38 |
| av. | 0.41 | 0.38 |

close to the formal value, though the Th s population is somewhat larger than the formal value of 0. In both **1** and **2** the d and f populations are significantly larger than their formal values, and it is these populations which are primarily responsible for the Mulliken charges on the metal atoms being so much less than 4. As such enhanced d and f populations would normally indicate the occupation of molecular orbitals with d and/or f character, we examined the compositions of the 51 highest occupied levels in both complexes. However, little evidence of significant metal contribution to these orbitals was found, with no more than 2% d and/or f character to any orbital of either **1** or **2**. Therefore, we conclude that there is little f-element−oxygen covalency in either **1** or **2**, and hence that the larger orbital term in the energy decomposition of **1** compared with **2** most likely reflects a stronger ionic component to the bonding.

The Mayer Bond Orders (MBOs) between the f-elements and the oxygens to which they are coordinated are given in Table 5. MBOs have a potential advantage over the analysis of the character of individual MOs in that they contain all of the contributions to a bond between two atoms, that is they take account of all bonding and antibonding interactions in a single number. It can be seen that all four values for **2** are very similar to one another, while there is slightly more variation in the Ce−O values. It is also apparent that the average MBO is slightly larger for **1** than for **2**, suggesting that the Ce−O bonds are slightly stronger than the Th−O, in agreement with the results from the energy decomposition scheme.

**(ii) Vibrational Spectroscopy.** ATR-IR were recorded for both the $Ce^{IV}$ and $Th^{IV}$ complexes in both the solid state and in aqueous solution. The observed IR vibrational bands of the $Ce^{IV}$ and $Th^{IV}$ complexes and that of the "free" ligand crystallized as a tetrabutylammonium salt, $(n\text{-}Bu_4N)_4H_3[PMo_{11}O_{39}]$ are detailed in the Supporting Information. They all exhibit characteristic asymmetric stretching vibrations in the P−O and Mo−O stretch regions.

The infrared spectrum of each complex (**1** and **2**) exhibited two bands in the P−O stretching region associated with vibrations within the phosphate ($\{PO_4\}^{3-}$) unit in the interior of the lacunary anion ligands, as previously described for the analogous trivalent lanthanide complexes.[12,13] These two bands in the "free" lacunary are split by about 27 $cm^{-1}$. However, on coordination to a metal center these two bands are split further, probably as a result of increased distortion and subsequent loss of symmetry at the phosphate center. In the spectrum of $[Ce(PMo_{11}O_{39})_2]^{10-}$ (**1**) the two P−O bands are split by 48 $cm^{-1}$ and in the $[Th(PMo_{11}O_{39})_2]^{10-}$ (**2**) by 43 $cm^{-1}$. The broad peak in the IR spectrum of **2** at 1400 $cm^{-1}$ is associated with ammonium counter cations.

When the splitting of the P−O band in the solid phase for the tetravalent complexes is compared to that in the analogous trivalent lanthanide complexes (see Supporting Information), the ionic radius of the metal appears to determine the magnitude of the splitting. The increased positive charge density and decreased ionic radius for $Ce^{IV}$ versus $Th^{IV}$ probably accounts for the larger splitting in $[Ce(PMo_{11}O_{39})_2]^{10-}$ versus $[Th(PMo_{11}O_{39})_2]^{10-}$, an effect previously observed for the analogous trivalent lanthanide complexes.[12,13] Interestingly, it would appear that both the $Th^{IV}$ and $Ce^{IV}$ complexes sit below the general trend of increasing P−O splitting with decrease in ionic radii observed for the series of $Ln^{III}$ complexes (although the differences observed are close to the resolution of the instrument). This would appear to be counter intuitive, as seen for the M−O bond length data discussed previously, with a stronger $Ln^{III}$−O interaction versus $Ce^{IV}/Th^{IV}$ interaction for comparable metal ionic radii. The solution phase measurements indicate a similar splitting to that of the solid state measurements with a splitting of 54 $cm^{-1}$ observed for the $Ce^{IV}$ complex and 40 $cm^{-1}$ for the $Th^{IV}$ complex, indicating that the two complexes are stable in solution.

The Raman spectra are less informative although $[Ce(PMo_{11}O_{39})_2]^{10-}$ and $[Th(PMo_{11}O_{39})_2]^{10-}$ both exhibit a band in the solid state Raman spectra associated with the $Mo-O_{terminal}$ symmetric stretching vibration (at 975 and 974 $cm^{-1}$, respectively), shifted to higher energy from the uncoordinated ligand (967 $cm^{-1}$). Two further bands attributed to the $Mo-O_{terminal}$ asymmetric stretch can be seen clearly in the $Th^{IV}$ compound at 955 and 925 $cm^{-1}$, which are only observed as shoulders in the spectrum of the $Ce^{IV}$ compound. The aqueous solution spectra of both complexes exhibit nearly identical features despite the lower spectral resolution, indicating the stability of the complex in solution.

**(iii) $^{31}$P NMR Spectroscopy.** $^{31}$P NMR spectra of **1** and **2** were recorded in $D_2O$, with the CP-MAS $^{31}$P NMR spectrum also collected for $Cs_{10}[Ce(PMo_{11}O_{39})_2]\cdot 26H_2O$ (unfortunately we did not have access to a facility that would allow us to undertake the comparable solid state Th measurement because of radiological safety considerations). Both complexes show only one sharp well resolved peak in solution: 2.55 ppm for the $Ce^{IV}$ complex and 2.52 ppm for the $Th^{IV}$ complex. These values can be compared to "uncoordinated" $[PMo_{11}O_{39}]^{7-}$, which has chemical shift of about 1 ppm (a peak slightly affected by the extent of protonation of the anion, and hence pH).[28] The small shift

(28) (a) Pettersson, L.; Andersson, I.; Öhman, L. O. *Inorg. Chem.* **1986**, *25*, 4726. (b) Combs-Walker, L. A.; Hill, C. L. *Inorg. Chem.* **1991**, *30*, 4016. (c) Himeno, S.; Hashimoto, M.; Ueda, T. *Inorg. Chim. Acta* **1999**, *284*, 237.

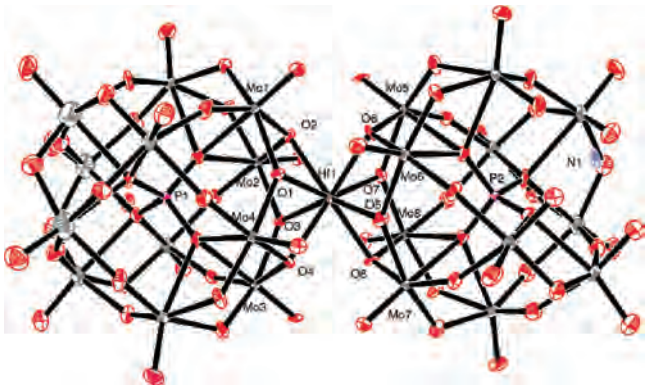


**Figure 3.** ORTEP representation (50% probability ellipsoids) of **3b**.

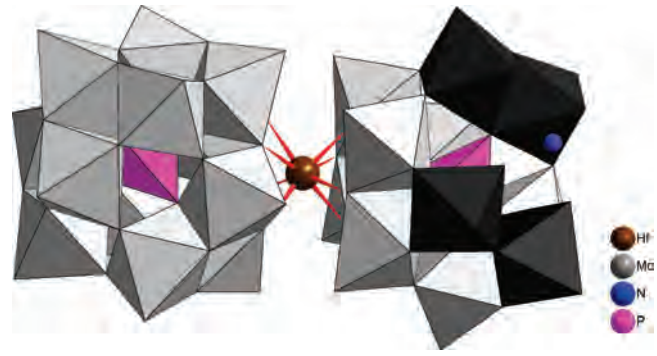


**Figure 4.** Polyhedral representation of **3b**, the darker shaded polyhedrons represent the Mo octahedra that have associated terminal unsaturated oxygen atoms.

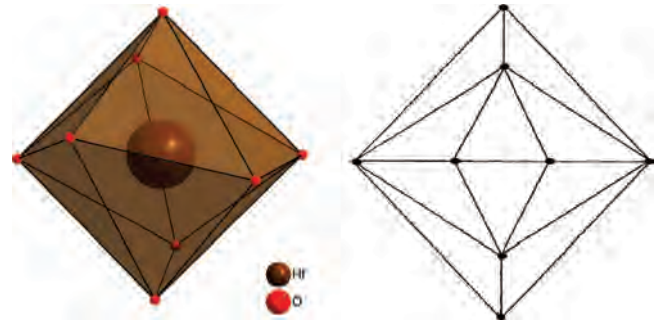


**Figure 5.** Polyhedral representation of the severely distorted triangular dodecahedral geometry around the central 8 coordinate $Hf^{IV}$ centre in **3b** and a sketch illustrating the traditional triangular dodecahedral geometry.

in the $^{31}P$ NMR signal on coordination to either $Ce^{IV}$ or $Th^{IV}$ is not surprising because the internal "phosphate" group is several bonds removed from the coordinated tetravalent metal centers and both metals are diamagnetic. Larger variation in chemical shifts were observed for the paramagnetic $Ln^{III}$ complexes previously studied. In comparison to the $Ce^{IV}$ complex, the related paramagnetic $Ce^{III}$ complex displays a $^{31}P$ chemical shift at about 7 ppm.[13] No peak in this region was observed for the $Ce^{IV}$ complex, so this is good evidence for the stabilization of the +IV oxidation state in solution. The $Ce^{IV}$ compound also only displays one peak in the solid state $^{31}P$ NMR spectrum at −3.40 ppm, again consistent with the presence of only one phosphorus environment in the compound.

As the pH of a $[PMo_{12}O_{40}]^{3-}$ solution is raised above pH 1 there is partial breakdown of the plenary anion to the lacunary anion, $[PMo_{11}O_{39}]^{7-}$. While there are other minor phosphomolybdate species present,[28] the only other dominating species is phosphate itself which is the major species above pH 5, with phosphomolybate undergoing complete breakdown through hydrolysis at near neutral pH (see Supporting Information). Both $[Ce(PMo_{11}O_{39})_2]^{10-}$ and $[Th(PMo_{11}O_{39})_2]^{10-}$ are stable over a wide pH range, dominating solution speciation between pH 1 to 5 at a 2:1 phosphomolybate:$Ce^{IV}$/$Th^{IV}$ ratio. There was no evidence for any interaction between $[PMo_{12}O_{40}]^{3-}$ and either tetravalent metal cation in solution, with any complexed peak expected to be close to the resonance for uncomplexed $[PMo_{12}O_{40}]^{3-}$ at about 3.7 ppm.[28]

**B. Hafnium(IV) and Zirconium(IV) Systems. (i) Crystallographic Characterization of $(NH_4)_5\{Hf[PMo_{12}O_{40}][(NH_4)PMo_{11}O_{39}]\}\cdot 23.5H_2O$.** The structure of the anion $\{Hf[PMo_{12}O_{40}][(NH_4)PMo_{11}O_{39}]\}^{5-}$ = **3b**, is shown in Figures 3 and 4, in ORTEP and polyhedral representations, respectively. Structural refinement located 23.5 water molecules per anionic cluster.

The complex contains an 8 coordinate hafnium cation complexed to one Keggin, $[PMo_{12}O_{40}]^{3-}$ anion and to one unsaturated lacunary, $[PMo_{11}O_{39}]^{7-}$ anion in a sandwich type complex. The Keggin anion is bonded to $Hf^{IV}$ via two corner shared and two edge shared bridging oxygen atoms. Interestingly, the lacunary anion, $[PMo_{11}O_{39}]^{7-}$, is also bonded to $Hf^{IV}$ through two corner shared and two edge shared bridging oxygen atoms and not through the four vacant terminal unsaturated oxygen atoms left available for bonding after the loss of $\{Mo{=}O\}^{4+}$ as might be expected. Instead the "hole" left after the degradation of the "parent" Keggin anion to the monovacant lacunary anion is occupied by an ammonium, $NH_4^+$, cation. To the best of our knowledge this is the first structurally characterized example where a coordinating metal cation prefers to bind to *non*-lacunary oxygens in a lacunary anion. The geometry around the central 8 coordinate $Hf^{IV}$ is best described as distorted triangular dodecahedron according to Haigh's rules (see Figure 5).[25] Selected bond distances and angles are detailed in Table 6.

The four bonds formed between $Hf^{IV}$ and the four bridging oxygen atoms of the lacunary anion, $[PMo_{11}O_{39}]^{7-}$, have an average distance of 2.19 Å. The bonds formed between the Keggin anion, $[PMo_{12}O_{40}]^{3-}$, and $Hf^{IV}$ also have an average bond distance of 2.19 Å. This is perhaps surprising because one might expect the lacunary anion to be bonded slightly closer to the metal because of the charge difference of −4 versus the Keggin anion. However, it is probable that the extra negative charge is largely localized around the lacunary site and therefore when $Hf^{IV}$ coordinates to a non-lacunary site it does so at a position where the charge density is very similar to that of the equivalent bridging oxygens of a Keggin anion. Each coordinated anion exhibits two long (O2, O4, O6, and O8) and two short (O1, O3, O5, and O7) bonds to $Hf^{IV}$, originating from edge shared and corner shared bridging oxygen atoms, respectively. The related $[Zr(PMo_{11}O_{39})(PMo_{12}O_{40})]^{6-}$ complex in which the lacunary anion is bonded through terminal oxygen atoms, exhibits an average

**Table 6.** Selected Bond Distances [Å] and Bond Angles [°] for Compound **3b**

| | | | | | |
|---|---|---|---|---|---|
| Hf(1)−O(1) | 2.149(9) | O(7)−Hf(1)−O(1) | 145.1(4) | O(3)−Hf(1)−O(8) | 85.1(3) |
| Hf(1)−O(3) | 2.150(9) | O(7)−Hf(1)−O(4) | 144.7(3) | O(7)−Hf(1)−O(2) | 84.2(3) |
| Hf(1)−O(2) | 2.240(9) | O(3)−Hf(1)−O(6) | 143.7(3) | O(5)−Hf(1)−O(4) | 83.0(3) |
| Hf(1)−O(4) | 2.228(9) | O(1)−Hf(1)−O(8) | 142.9(3) | O(1)−Hf(1)−O(6) | 81.2(3) |
| Hf(1)−O(5) | 2.156(9) | O(8)−Hf(1)−O(2) | 142.9(3) | O(8)−Hf(1)−O(4) | 76.3(3) |
| Hf(1)−O(7) | 2.143(9) | O(5)−Hf(1)−O(2) | 141.2(3) | O(2)−Hf(1)−O(6) | 75.4(3) |
| Hf(1)−O(6) | 2.259(9) | O(4)−Hf(1)−O(6) | 139.6(3) | O(5)−Hf(1)−O(8) | 70.6(3) |
| Hf(1)−O(8) | 2.210(9) | O(4)−Hf(1)−O(2) | 117.7(3) | O(7)−Hf(1)−O(8) | 70.5(3) |
| | | O(8)−Hf(1)−O(6) | 117.6(3) | O(3)−Hf(1)−O(2) | 70.2(3) |
| | | O(3)−Hf(1)−O(5) | 147.3(3) | O(1)−Hf(1)−O(4) | 70.0(3) |
| | | O(1)−Hf(1)−O(3) | 97.4(4) | O(3)−Hf(1)−O(4) | 69.9(3) |
| | | O(7)−Hf(1)−O(5) | 96.6(4) | O(1)−Hf(1)−O(2) | 69.9(3) |
| | | O(7)−Hf(1)−O(3) | 95.4(3) | O(7)−Hf(1)−O(6) | 69.5(3) |
| | | O(1)−Hf(1)−O(5) | 89.9(4) | O(5)−Hf(1)−O(6) | 68.9(3) |

bond distance to the $[PMo_{12}O_{40}]^{3-}$ anion of 2.22 Å and to the terminally bonded $[PMo_{11}O_{39}]^{7-}$ anion of 2.18 Å and an overall 8 coordinate average bond length of 2.20 Å.[14]

Although the structurally characterized hafnium and zirconium sandwich complexes both stabilize a Keggin anion and a lacunary anion (bound via bridging and terminal oxygen atoms, respectively) the average 8 coordinate bond distance is considerably shorter than the analogous tetravalent f-element complexes (**1** and **2**). This feature, which is irrespective of $[PMo_{11}O_{39}]^{7-}$/$[PMo_{12}O_{40}]^{3-}$ complexation, can best be explained by the smaller ionic radii and higher charge density of the tetravalent group 4d and 5d transition metal cations versus the 4f and 5f metal cations.

**(ii) Vibrational Spectroscopy.** Solid ATR-infrared spectra of the bulk solid of **3a** and the single crystals, **3b**, were recorded (Figure 6), as was the solution ATR-IR of the bulk solid dissolved in water. However, there were insufficient single crystals for solution analysis of **3b**.

Both bulk solid and crystals of **3** display IR bands associated with $Mo-O_{terminal}$, $Mo-O_{corner\text{-}shared}$, and $Mo-O_{edge\text{-}shared}$ vibrations in the 1000−700 $cm^{-1}$ region of the spectrum and also features associated with the ammonium counter cations (ca. 1415 $cm^{-1}$) and water molecules of crystallization (ca. 1610 $cm^{-1}$). However, the most distinctive P−O stretching region of the spectrum exhibits different features for the bulk solid and single crystals. Analysis of the small quantity of single crystals of **3b** by IR reveals three bands at 1061, 1027, and 1005 $cm^{-1}$. The bands at 1061 and 1005 $cm^{-1}$ are assigned to the two $\nu_{sym}$(P−O) stretches of the lacunary anion in local $C_{3v}$ symmetry resulting in a splitting of 56 $cm^{-1}$. The band at 1027 $cm^{-1}$ is assigned to the $\nu_{sym}$(P−O) stretch in the Keggin anion, shifted by 40 $cm^{-1}$ from "uncoordinated" Keggin. There is no evidence that this band is split into two on coordination. The bulk solid of **3** (**3a**) however exhibits four bands at 1110, 1060, 1030, and 1026 $cm^{-1}$, very similar to the four bands recorded at 1109, 1066, 1042, and 1026 $cm^{-1}$ for the related $Zr^{IV}$ complex reported previously.[14] The $Zr^{IV}$ complex was then prepared again in an analogous manner to the preparation of the bulk solid of the $Hf^{IV}$ complex (**3a**), again yielding a near identical spectrum to this bulk $Hf^{IV}$ material. Therefore, it is presumed that the bulk material is the same as that of the $Zr^{IV}$ species, in which two bands were assigned to the lacunary anion at 1109 and 1026 $cm^{-1}$ and the remaining two bands to the Keggin anion. If this assumption is correct then the P−O band in the lacunary anion is split by 81 $cm^{-1}$ and the Keggin anion by 34 $cm^{-1}$ in **3a**. It is also proposed that coordination through the terminal $[PMo_{11}O_{39}]^{7-}$ lacunary oxygens to $Zr^{IV}$ or $Hf^{IV}$ (**3a**) is the major structural product with coordination through bridging $[PMo_{11}O_{39}]^{7-}$ lacunary oxygens to $Hf^{IV}$ (**3b**) a minor product that fortuitously yields diffraction quality crystals.

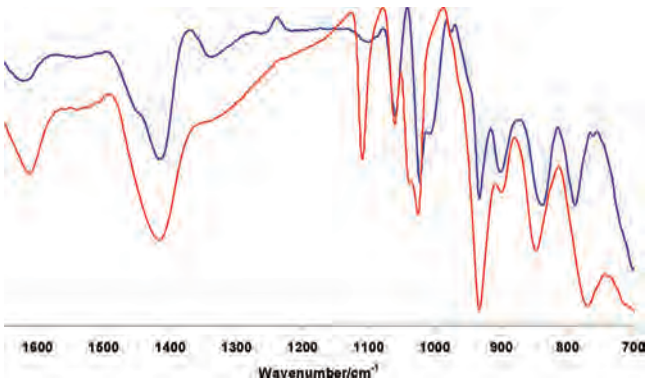


**Figure 6.** Solid IR spectrum of the $Hf^{IV}$ bulk solid (**3a**, red) and single crystals (**3b**, blue).

Solution ATR-IR was also performed on the bulk $(NH_4)_6[Hf(PMo_{11}O_{39})(PMo_{12}O_{40})]$ solid dissolved in $H_2O$. Although the spectrum was of low resolution it did reveal P−O bands at 1111, 1062, and 1030 $cm^{-1}$, similar to that observed in the solid state. Solid and solution Raman spectroscopy was used to probe the $Mo-O_{terminal}$ stretching frequencies within the Keggin and lacunary anion in a bulk solid sample containing $[Hf(PMo_{11}O_{39})(PMo_{12}O_{40})]^{6-}$. Two distinct bands were apparent in the solid Raman spectrum at 979 and 962 $cm^{-1}$, with two much smaller bands centered on 901 and 861 $cm^{-1}$. The solution spectrum was of much lower resolution, but displayed a large band at 979 $cm^{-1}$ and also a smaller band with an additional shoulder centered on 956 $cm^{-1}$. All bands can be attributed to Mo−O vibrations.

**(iii) $^{31}$P NMR Spectroscopy.** Solid state CP-MAS $^{31}$P NMR spectroscopy was performed on the bulk $Hf^{IV}$ compound (**3a**) and the analogous (from IR spectroscopy) $Zr^{IV}$ complex (see Supporting Information). As both complexes contain coordinated $[PMo_{11}O_{39}]^{7-}$ and $[PMo_{12}O_{40}]^{3-}$ then two peaks of equal intensity would be expected, which is what is observed; at −1.38 and −4.34 ppm for the $Hf^{IV}$ system and −1.53 and −4.16 ppm for the $Zr^{IV}$ system. The peak at about −1 ppm is attributed to a coordinated lacunary anion

with the peak at about −4 ppm attributed to coordinated Keggin anion. If the $Hf^{IV}$ complex was stable in solution then a similar spectrum would be expected.

However, the solution spectrum of the bulk solid dissolved in $D_2O$ displays three $^{31}P$ NMR signals at 1.37, −1.42, and −1.68 ppm (see Supporting Information). We had previously reported a complex $^{31}P$ NMR spectrum for the $Zr^{IV}$ system which indicates that perhaps neither $[Hf(PMo_{11}O_{39})(PMo_{12}O_{40})]^{6-}$ nor $[Zr(PMo_{11}O_{39})(PMo_{12}O_{40})]^{6-}$ are stable in solution.[14]

**(iv) Solution State $^{31}P$ NMR Study of the $Zr^{IV}$ and $Hf^{IV}$ in the Presence of Phosphomolybdate as a Function of pH.** In an attempt to elucidate $[PMo_{11}O_{39}]^{7-}$/$[PMo_{12}O_{40}]^{3-}$ complexation to $Hf^{IV}$/$Zr^{IV}$ in solution, $^{31}P$ NMR spectra were recorded at a 2:1 phosphomolybdate:Group 4 metal cation ratio as a function of increasing pH (see Supporting Information). The speciation in both the $Hf^{IV}$ and $Zr^{IV}$ cases are very similar and distinct from the behavior observed for the $Ce^{IV}$ (**1**) and $Th^{IV}$ (**2**) systems. Initially on elevation of pH a signal indicative of a species incorporating the Keggin anion appears at −3.5 and −3.2 ppm for $Hf^{IV}$ and $Zr^{IV}$, respectively, and a small amount of "free" Keggin is also apparent at −3.7 ppm, which disappears on further elevation of pH. The dominant feature in solution is this Keggin complex up to approximately pH 2 when two peaks very close to each other begin to grow into the spectrum between −1.5 and −2.0 ppm for both $Hf^{IV}$ and $Zr^{IV}$ systems. These two new peaks are in the lacunary, $[PMo_{11}O_{39}]^{7-}$ region of the spectrum and continue to grow in intensity until they reach a maximum at approximately pH 4.5−4.9. The Keggin signal is present in solution up to a pH of approximately 4.3−4.6 for both metals, after which the two lacunary signals dominate until breaking down to $[PO_4]^{3-}$ and $[MoO_4]^{2-}$ above pH 5.3 (only shown in the Supporting Information for the $Zr^{IV}$ system).

From the $^{31}P$ NMR spectra, speciation at low pH is dominated by a complex between the stabilized Keggin anion and the tetravalent metal, which is probably a 2:1 sandwich complex. As the pH is increased further, a mechanism must take place in which Keggin anions undergo degradation to lacunary anions, which can also complex to the tetravalent metal. The formation of the two peaks in the lacunary region at equivalent intensity perhaps indicates the formation of a 2:1 $[PMo_{11}O_{39}]^{7-}$:$Zr^{IV}$/$Hf^{IV}$ complex with one lacunary anion bound through terminal oxygens at the defect site (as is normally the case for lacunary anion complexation) and the other bound through bridging oxygens (as observed in **3b**). It is rather puzzling that the spectra do not support the stabilization of a mixed lacunary/Keggin complex as a major species. For this to be the case we would expect to see two peaks of equivalent intensity, one in the lacunary region and one in the Keggin region of a solution spectrum at a given pH (as observed in the CP-MAS spectra). However, the spectra do confirm the ability of both $Zr^{IV}$ and $Hf^{IV}$ to stabilize $[PMo_{12}O_{40}]^{3-}$ to a much higher pH than is usually observed. In addition, it should be noted that the spectrum of the bulk $Hf^{IV}$ complex (**3a**) dissolved in $D_2O$ (discussed previously) is similar to the phosphomolybdate:$Hf^{IV}$ spectrum recorded at pH 5.20 and also the phosphomolybdate:$Zr^{IV}$ spectrum recorded at pH 5.30.

**Table 7.** PBE Energy Decomposition Data (eV) for **3a**, $Hf(PMo_{11}O_{39})(PMo_{12}O_{40})^{6-}$, and **4a**, $Zr(PMo_{11}O_{39})(PMo_{12}O_{40})^{6-}$, at the Crystallographic Coordinates of **4a**[14]

| | $Zr(PMo_{11}O_{39})(PMo_{12}O_{40})^{6-}$ | $Hf(PMo_{11}O_{39})(PMo_{12}O_{40})^{6-}$ |
|---|---|---|
| electrostatic | −85.26 | −86.25 |
| Pauli | 15.32 | 15.36 |
| prerelaxation (= electrostatic + Pauli) | −69.94 | −70.89 |
| orbital | −46.93 | −46.43 |
| total bonding energy | −116.87 | −117.32 |

**(v) Computational Analysis of the Metal−POM Interactions in $[M(PMo_{11}O_{39})(PMo_{12}O_{40})]^{6-}$ (where M = Zr - 4a, Hf - 3a) and $\{Hf[PMo_{12}O_{40}][(NH_4)PMo_{11}O_{39}]\}^{5-}$ (where M = Zr - 4b, Hf - 3b).** LDA geometry optimizations of $[Zr(PMo_{11}O_{39})(PMo_{12}O_{40})]^{6-}$, conducted without symmetry constraints and starting from the crystallographic coordinates, did not converge. Therefore, we decided to probe the metal-POM interactions via a single point PBE calculation at the crystallographic coordinates, and to compare Zr with Hf by conducting an analogous calculation on the latter system using the coordinates of the Zr anion. As for **1** and **2**, we have analyzed the metal−POM interactions using the energy decomposition scheme, partial charges, Mulliken atomic populations, and MBOs.

Energy decomposition data for $[M(PMo_{11}O_{39})(PMo_{12}O_{40})]^{6-}$ (M = Zr, Hf), using a three-fragment division ($M^{4+}$/$(PMo_{11}O_{39})^{7-}$/$(PMo_{12}O_{40})^{3-}$), are given in Table 7. It is immediately apparent that the two sets of data are very similar to one another, the largest difference being 0.99 eV in the electrostatic term, with the total bonding energies lying within 0.45 eV of one another (less than 0.5%). As with **1** and **2**, the dominant term in the energy decomposition of $[M(PMo_{11}O_{39})(PMo_{12}O_{40})]^{6-}$ (M = Zr, Hf) is the electrostatic term, although it is smaller than in the f-element compounds on account of the reduced negative charge of the ligand environment.

Mulliken, Voronoi, and Hirshfeld partial charges of the metal atoms, and the oxygens to which they are coordinated, were collected for **4a**, **3a**, **4b**, and **3b** in Table 8. Focusing first on **4a** and **3a**, all three schemes indicate that the charges on O1−O4 (Keggin) are more negative than on O5−O8 (lacunary), with the Voronoi and Hirshfeld values being very similar to one another, and much smaller than the Mulliken, as noted for **1** and **2**. For the metal charges, both Voronoi and Hirshfeld indicate that the charge on Hf is slightly more positive than for Zr, while the Mulliken charge for Hf is substantially lower than that for Zr. The charge difference between metal and oxygens is large in all cases, suggestive of significant ionicity, as noted for **1** and **2**. Interestingly, for **4b** and **3b** the difference between the partial charges of O1−O4 and O5−O8 disappears, with all eight coordinating oxygens having rather similar charges. However, there is no consistent pattern as to which **4a/3a** oxygens those in **4b** and **3b** resemble most closely. The Voronoi and Hirshfeld approaches suggest that all eight **4b** oxygens carry a similar charge to the Keggin oxygens in **4a**, while for **3b** these

**Table 8.** PBE Partial Atomic Charges for **4a**, **3a**, **4b**, and **3b**

| | Mulliken | | | | Voronoi | | | | Hirshfeld | | | |
|---|---|---|---|---|---|---|---|---|---|---|---|---|
| | **4a** | **3a** | **4b** | **3b** | **4a** | **3a** | **4b** | **3b** | **4a** | **3a** | **4b** | **3b** |
| O1 | −0.92 | −0.91 | −0.84 | −0.79 | −0.35 | −0.35 | −0.33 | −0.29 | −0.35 | −0.35 | −0.33 | −0.30 |
| O2 | −0.86 | −0.85 | −0.80 | −0.75 | −0.32 | −0.32 | −0.32 | −0.29 | −0.33 | −0.33 | −0.31 | −0.28 |
| O3 | −0.92 | −0.91 | −0.84 | −0.78 | −0.35 | −0.35 | −0.33 | −0.29 | −0.31 | −0.32 | −0.33 | −0.29 |
| O4 | −0.89 | −0.88 | −0.80 | −0.75 | −0.34 | −0.34 | −0.33 | −0.30 | −0.35 | −0.35 | −0.31 | −0.29 |
| O5 | −0.82 | −0.81 | −0.84 | −0.78 | −0.27 | −0.27 | −0.33 | −0.28 | −0.27 | −0.27 | −0.33 | −0.29 |
| O6 | −0.82 | −0.82 | −0.80 | −0.74 | −0.26 | −0.27 | −0.33 | −0.29 | −0.27 | −0.27 | −0.32 | −0.28 |
| O7 | −0.82 | −0.81 | −0.84 | −0.78 | −0.27 | −0.27 | −0.34 | −0.29 | −0.27 | −0.27 | −0.34 | −0.29 |
| O8 | −0.82 | −0.82 | −0.81 | −0.75 | −0.26 | −0.27 | −0.34 | −0.29 | −0.27 | −0.27 | −0.33 | −0.28 |
| M | 1.95 | 1.55 | 1.77 | 0.60 | 0.47 | 0.52 | 0.40 | 0.24 | 0.55 | 0.59 | 0.43 | 0.27 |

**Table 9.** PBE Mulliken Population Analysis of **4a**, **3a**, **4b**, and **3b**

| | **4a** | | | | **3a** | | | | **4b** | | | | **3b** | | | |
|---|---|---|---|---|---|---|---|---|---|---|---|---|---|---|---|---|
| | s | p | d | f | s | p | d | f | s | p | d | f | s | p | d | f |
| O1 | 2.00 | 4.89 | 0.03 | 0.0 | 2.00 | 4.89 | 0.03 | 0.0 | 2.01 | 4.80 | 0.03 | 0.0 | 2.01 | 4.74 | 0.03 | 0.0 |
| O2 | 2.01 | 4.81 | 0.03 | 0.0 | 2.01 | 4.81 | 0.03 | 0.0 | 2.02 | 4.74 | 0.03 | 0.0 | 2.02 | 4.69 | 0.03 | 0.0 |
| O3 | 2.00 | 4.89 | 0.03 | 0.0 | 2.00 | 4.89 | 0.03 | 0.0 | 2.02 | 4.79 | 0.03 | 0.0 | 2.02 | 4.73 | 0.03 | 0.0 |
| O4 | 2.01 | 4.85 | 0.03 | 0.0 | 2.01 | 4.85 | 0.03 | 0.0 | 2.02 | 4.74 | 0.03 | 0.0 | 2.02 | 4.70 | 0.03 | 0.0 |
| O5 | 2.05 | 4.73 | 0.03 | 0.0 | 2.05 | 4.73 | 0.03 | 0.0 | 2.01 | 4.79 | 0.03 | 0.0 | 2.02 | 4.73 | 0.04 | 0.0 |
| O6 | 2.04 | 4.75 | 0.03 | 0.0 | 2.04 | 4.75 | 0.03 | 0.0 | 2.02 | 4.75 | 0.04 | 0.0 | 2.02 | 4.69 | 0.04 | 0.0 |
| O7 | 2.05 | 4.73 | 0.03 | 0.0 | 2.05 | 4.73 | 0.03 | 0.0 | 2.01 | 4.80 | 0.03 | 0.0 | 2.02 | 4.73 | 0.03 | 0.0 |
| O8 | 2.04 | 4.75 | 0.03 | 0.0 | 2.04 | 4.75 | 0.03 | 0.0 | 2.02 | 4.76 | 0.03 | 0.0 | 2.02 | 4.69 | 0.03 | 0.0 |
| M | 0.31 | 0.18 | 1.56 | 0.0 | 0.50 | 0.23 | 1.69 | 14.04 | 0.80 | 0.29 | 0.95 | 0.2 | 1.62 | 0.31 | 1.14 | 14.32 |

schemes yield oxygen charges closer to the lacunary oxygens of **3a**. The Mulliken charges for the oxygens in both **3b** and **4b** are closer to the lacunary values for **4a** and **3a**. All three charge schemes agree in finding metal charges in **4b** and **3b**, which are smaller than in the systems without the ammonium ion. This reduction in charge on ammonium coordination is larger for Hf than for Zr, particularly for the Mulliken charge.

Mulliken atomic populations are given in Table 9. Formally, $Zr^{4+}$ has the configuration $ns^0np^0(n-1)d^0$, where $n = 5$, while for $Hf^{4+}$ the formal configuration is $ns^0np^0(n-1)d^0(n-2)f$,[14] $n = 6$. In $[M(PMo_{11}O_{39})(PMo_{12}O_{40})]^{6-}$ (M = Zr, Hf), all of the metals' atomic populations are larger than the formal value, in agreement with the observed metal charges being very much less than the formal value. The Hf s, p and d populations are all larger than the corresponding Zr values, and both the Zr and Hf s, p and d populations are larger than those calculated for the metals in **1** and **2**. However, as with **1** and **2**, examination of the highest 51 molecular orbitals of **3a** and **4a** reveals little metal character, with no more than 2% d contribution to a handful of levels. These data suggest that, as with the f-element systems, there is rather little Zr/Hf−oxygen covalency.

The Mulliken populations of **4b** and particularly **3b** show a large s population on the central metal. In the Hf case, the large s population is clearly the cause of the small Hf Mulliken charge noted above. We examined the highest 51 occupied MOs for large s contributions but, as with the d character in **4a** and **3a**, little evidence was found, other than some non-negligible but negative contributions from the formally unoccupied Hf 6s orbital. Such s contributions are not unknown for anionic systems with medium to large basis sets, but why this should be the case only in **3b** of the present targets is not clear.

As with **1** and **2** but probably more so, we do not consider the Mulliken population and charge data for the Zr and Hf systems to be very reliable. Not only are the latter rather anionic, but none of the systems are being studied at their optimized geometry, and none has any symmetry to aid analysis.

**Table 10.** PBE Zr/Hf−O Mayer Bond Orders of **4a**, **3a**, **4b**, and **3b**; O1−O4 Are from the Keggin Ligand

| | **4a** | **3a** | **4b** | **3b** |
|---|---|---|---|---|
| O1 | 0.36 | 0.41 | 0.24 | 0.19 |
| O2 | 0.25 | 0.25 | 0.16 | 0.13 |
| O3 | 0.24 | 0.23 | 0.15 | 0.13 |
| O4 | 0.51 | 0.41 | 0.25 | 0.20 |
| Av. | 0.34 | 0.33 | 0.20 | 0.16 |
| O5 | 0.41 | 0.46 | 0.20 | 0.15 |
| O6 | 0.38 | 0.45 | 0.31 | 0.23 |
| O7 | 0.41 | 0.46 | 0.20 | 0.15 |
| O8 | 0.51 | 0.45 | 0.28 | 0.20 |
| Av. | 0.43 | 0.46 | 0.25 | 0.18 |

The Zr/Hf−O MBOs are given in Table 10. For all four compounds, the average MBOs are larger for the lacunary ligand than for the Keggin and, for **4a** and **3a**, the average MBOs to the Keggin ligand are less than in **1** and **2** while those to the lacunary anions are larger. In all cases bar the lacunary in **4a** and **3a**, the Zr−O MBOs are larger than the Hf−O MBOs. There is a noticeably larger variation in the MBOs to the Keggin ligands in **4a** and **3a** than to the lacunary. In **1** and **2** the MBOs supported the energy decomposition data in suggesting stronger Ce−O interactions than Th−O interactions. It may be that the data in Table 10 indicate that the bonding to the central metal is weakened on complexation by $NH_4^+$, but in the absence of energy decomposition data for **4b** and **3b** we cannot be sure.

## Conclusions

Both $Th^{IV}$ and $Ce^{IV}$ react with phosphomolydate to form the classical lacunary sandwich complexes, $[Ce(PMo_{11}O_{39})_2]^{10-}$ and $[Th(PMo_{11}O_{39})_2]^{10-}$, respectively, with coordination to the f-block cations via the four terminal unsaturated oxygens of each ligand. Both complexes are

stable in solution over a wide pH range. In contrast, despite undertaking the reaction at the optimum pH range for $[PMo_{11}O_{39}]^{7-}$ formation the analogous complexes cannot be prepared for $Zr^{IV}$ or $Hf^{IV}$. Instead the major product contains both coordinated lacunary, $[PMo_{11}O_{39}]^{7-}$, and plenary Keggin, $[PMo_{12}O_{40}]^{3-}$, anions. From comparison with the previously structurally characterized $Zr^{IV}$ complex the major solid state product in both the $Zr^{IV}$ and $Hf^{IV}$ systems involves coordination to the four terminal unsaturated oxygens of $[PMo_{11}O_{39}]^{7-}$ and four bridging oxygens of $[PMo_{12}O_{40}]^{3-}$, that is, $[M(PMo_{11}O_{39})(PMo_{12}O_{40})]^{6-}$ (where M = Zr or Hf). Crystallization of a minor product from the $Hf^{IV}$ system yielded a complex containing the anionic cluster $\{Hf[PMo_{12}O_{40}][(NH_4)PMo_{11}O_{39}]\}^{5-}$. In this case the $Hf^{IV}$ cation does not bind to the terminal unsaturated oxygens of $[PMo_{11}O_{39}]^{7-}$, instead coordinating to two corner shared and two edge shared bridging oxygens. While solution $^{31}P$ NMR spectroscopy does indicate that the mixed complexes are stable in solution they do show that both $Zr^{IV}$ and $Hf^{IV}$ can stabilize $[PMo_{12}O_{40}]^{3-}$ to much higher pH values than usually observed and that $[PMo_{11}O_{39}]^{7-}$ coordination still occurs at higher pH values.

Density functional analysis of **1**(Ce) and **2**(Th) proved rather more successful than on the Zr and Hf containing systems. For the f-element complexes, bond energy decomposition, and MBOs suggest that the Ce−O bond is stronger than the Th−O, in agreement with the shorter Ce−O bond lengths. Little evidence is found for metal−oxygen covalency. Although calculations on the transition metal systems were less successful, they also point to very ionic interactions between the central metal and the surrounding oxygens.

Neither the experimental (spectroscopic and structural) nor the computational results could provide any clear answers as to why the $Zr^{IV}$ and $Hf^{IV}$ phosphomolybdate systems behave so differently to the $Ce^{IV}$ and $Th^{IV}$ phosphomolybdate systems. In fact, we have shown that $Zr^{IV}$ and $Hf^{IV}$ interactions with phosphomolybdate are even more complex than we had previously thought. This is in stark contrast to the phosphotungstate system where both $[Zr(PW_{11}O_{39})_2]^{10-}$and $[Hf(PMo_{11}O_{39})_2]^{10-}$ can be readily prepared, perhaps reflecting the greater stability of $[PW_{11}O_{39}]^{7-}$ versus $[PMo_{11}O_{39}]^{7-}$.

**Acknowledgment.** We are grateful to the EPSRC for financial support for L.J. (Grant EP/C543300/1) and D.D. (Grant EP/C013360/1) and the EPSRC and Nexia Solutions (and The Nuclear Decommissioning Authority) for a CASE studentship for R.C. We also acknowledge the Heavy Element Chemical Research Program, Chemical Sciences Division of the Office of Basic Energy Sciences, United States Department of Energy and the Los Alamos Laboratory Directed Research and Development Program for current funding (I.M.).

**Supporting Information Available:** This material is available free of charge via the Internet at http://pubs.acs.org.

IC800101T